Available online at www.sciencedirect.com
SCIENCE DIRECT®
Advances in Space Research 35 (2005) 1012–1016
ADVANCES IN SPACE RESEARCH (a COSPAR publication)
www.elsevier.com/locate/asr

Multi-phase interstellar clouds in the Vela SNR resolved with XMM-Newton

M. Miceli [a,*], F. Bocchino [b], A. Maggio [b], F. Reale [a]

[a] Dipartimento di Scienze Fisiche ed Astronomiche, Sezione di Astronomia, Università di Palermo, Piazza del Parlamento 1, 90134 Palermo, Italy
[b] INAF – Osservatorio Astronomico di Palermo, Piazza del Parlamento 1, 90134 Palermo, Italy

Received 24 September 2004; received in revised form 21 December 2004; accepted 24 December 2004

Abstract

XMM-Newton spatial/spectral resolution and high effective area allow to deepen our knowledge about the shocks in Supernova Remnants and their interaction with the interstellar medium. We present the analysis of an EPIC observation of the northern rim of the Vela SNR and we compare the X-ray and optical morphology of the emission. We derive a description of the internal structure of the shocked interstellar clouds, arguing that the transmitted shock model is compatible with our data. We also suggest that thermal conduction between clouds and inter-cloud medium is very efficient and produces the evaporation of the clouds in the interstellar medium.

Keywords: X-rays: ISM; Supernova remnants; Vela SNR

1. Introduction and data

The evolution of Supernova Remnants (SNRs) is deeply influenced by their interaction with the inhomogeneities of the ambient medium which affect the speed and the direction of the expanding shock wave. The interaction of the shock with the clouds of the interstellar medium (ISM) produces the characteristic, patchy X-ray morphology and the filamentary optical emission of middle-aged SNRs.

From the analysis of optical and X-ray observations, three different physical scenarios have been suggested to explain the details of the shock–cloud interaction and of the observed emission. These scenarios all associate the optical emission with a transmitted shock which travels through the clouds, while the X-ray emission is associated: (i) with the evaporation of the clouds engulfed by the main blast wave (Fesen et al., 1982; Charles et al., 1985; Bocchino and Bandiera, 2003); (ii) with a reflected shock which further heats the shocked inter-cloud medium [1] (Graham et al., 1995; Levenson et al., 1996; Miyata and Tsunemi, 2001); (iii) with a transmitted shock which propagates through inhomogeneities with an inward increasing density profile (Bocchino et al., 2000; Patnaude et al., 2002; Levenson et al., 2003).

The Vela SNR is the nearest middle-aged SNR (distance ~ 280 pc, Bocchino et al., 1999; Cha et al., 1999) so it is an ideal laboratory for a detailed study of the shock–cloud interaction which could allow one to discriminate between the three models.

In this paper, we discuss the analysis of an *XMM-Newton* EPIC observation of the northern rim of the Vela SNR. The observed region lies just behind the main shock front and, as shown by a previous ROSAT PSPC

* Corresponding author. Tel.: +39 91 233 111.
E-mail address: miceli@astropa.unipa.it (M. Miceli).

[1] The almost uniform component of the ISM which surrounds the clouds.

0273-1177/$30 © 2005 COSPAR. Published by Elsevier Ltd. All rights reserved.
doi:10.1016/j.asr.2004.12.065

observation (Bocchino et al., 1999), in this part of the shell there is a clear signature of the interaction of the shock with a relatively small and isolated cloud, named FilD. The aims of our work are: (i) to obtain a detailed description of the ISM clouds and of their internal structure; (ii) to obtain information about the physical properties of the shocked plasma, and (iii) to study the dynamics and evolution of the shock–cloud interaction.

Our data consist of a Guaranteed Time EPIC observation with pointing coordinates α (2000) = $8^h35^m44^s$, δ (2000) = $-42°35'29''$. We performed a time screening to eliminate the time intervals contaminated by soft-proton flares (characterized by rapid and strong variability in the light curve); the screened exposure times are 11.5 ks, for pn data, and 25.2 ks, for MOS1 and MOS2 data. We used the medium filter and the Extended Full Frame Mode (for pn) and the Large Window Mode (for MOS1 and MOS2).

2. Structure and physical parameters of the shocked clouds

Fig. 1 (top panel) shows the EPIC adaptively smoothed and vignetting corrected count rate image in the 0.3–10 keV energy band. The structure in the center of the field of view, composed of two bright knots, is the FilD cloud. At North-East another bright structure (named RegNE) is visible. The X-ray emission of FilD is quite soft (below 0.5 keV) while RegNE has a harder emission (almost entirely concentrated in the 0.5–1 keV band).

There is a clear relationship between the optical and X-ray emission in the FilD knot. Fig. 1 (bottom panel) shows a DSS archive image of the FilD region where the optical filament studied by Bocchino et al. (2000) is visible (near the bright star in the center of the image). We have superimposed the X-ray contour levels in the 0.3–0.5 keV band. The optical filament lies just between the two FilD regions (indicated with "a" and "b" in the top panel of Fig. 1) with the highest X-ray surface brightness. This relationship, observed also in the Cygnus Loop by Patnaude et al. (2002), suggests that the optical filaments represent the inner and denser part of the FilD cloud.

We studied in detail the distribution of the physical parameters of the post-shock plasma performing a spatially resolved spectral analysis (for the details of our analysis, see Miceli et al., submitted for publication). We analyzed the spectra extracted from 16 subregions (indicated in Fig. 2, top panel) which cover the whole FilD cloud, RegNE, the bright structure at the South-West and the dark area at the North. The subregions have an extension of a few arcminutes and in each subregion the mean photon energy can be considered almost uniform; in fact the mean photon energy in the pixels of any given subregion presents fluctuations <4%.

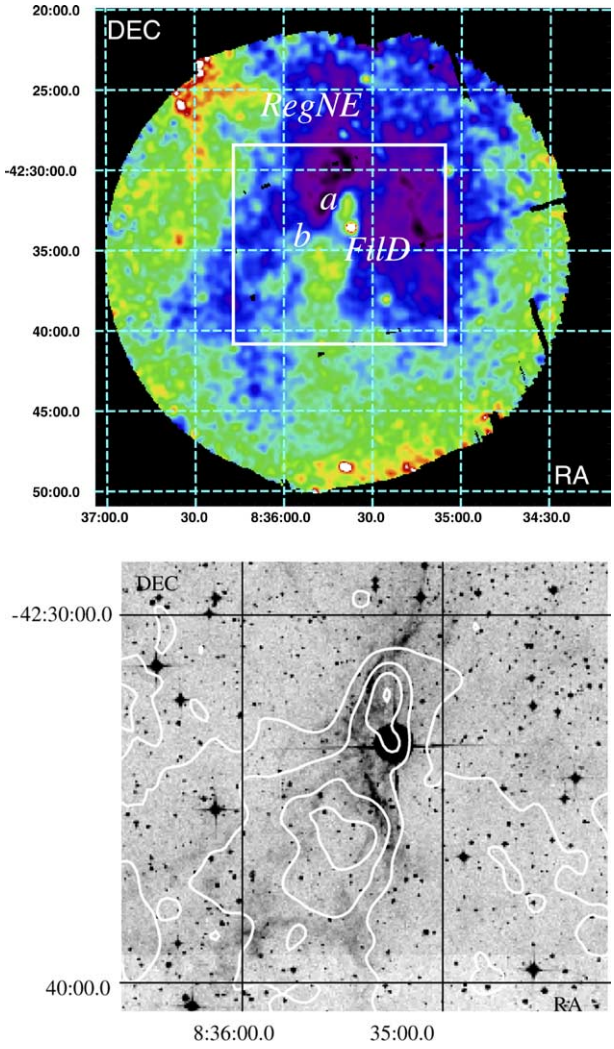

Fig. 1. *Top panel:* Adaptively smoothed count rate image in the 0.3–10 keV band. This image is a weighted average of the pn, MOS1 and MOS2 images (and is expressed in MOS-equivalent count rate), the bin size is 4″, North is up and East is on the left. *Bottom panel:* DSS archive image of the FilD region, the field of view is indicated by the white square shown in the left panel. We have superimposed (in white) 7 X-ray contour levels (equispaced between 0 and 7.1×10^{-5} cnt s^{-1} bin^{-1}) in the 0.3–0.5 keV band. The bright star is the optical counterpart of the X-ray point-like source visible in the left panel; this source is not related to the Vela SNR.

A single temperature model both in CIE or NEI is rejected in all the regions except for RegNE. All spectra are described (at 95% confidence level) by two MEKAL components of an optically-thin thermal plasma (Mewe et al., 1985, 1986; Liedahl et al., 1995). The fits with the PSHOCK non-equilibrium ionization model (Borkowski et al., 2001) do not significantly improve the quality of the fits and the best-fit τ_{NEI} values indicate that the plasma has already reached collisional ionization equilibrium. Fig. 2 (bottom panel) shows a representative spectrum together with its best-fit model. The temperature of each component is rather uniform in the field of view and is not related with the X-ray surface

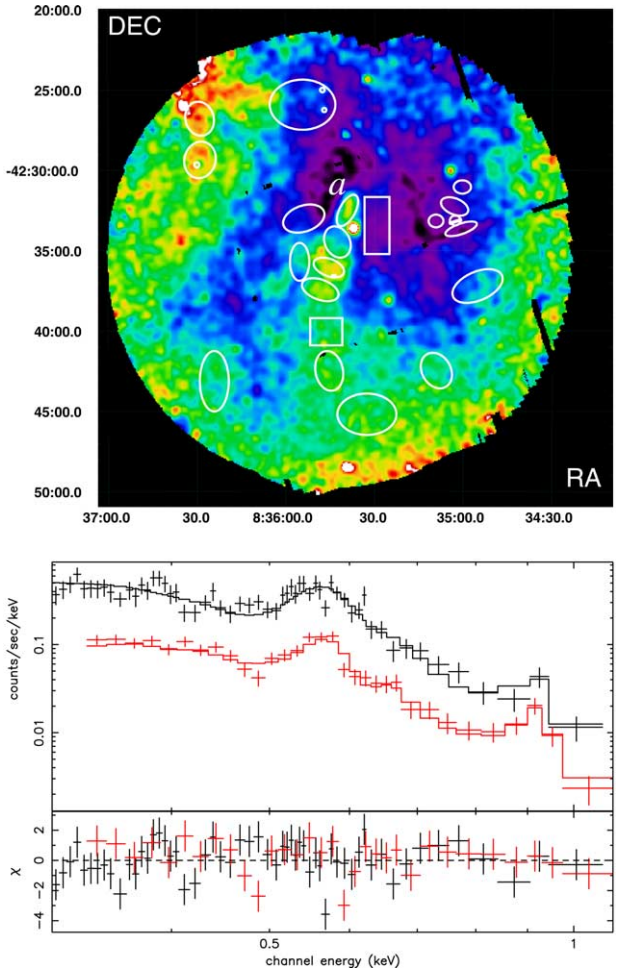

Fig. 2. *Top panel:* Same as Fig. 1 (left panel). The 16 subregions selected for spectral analysis are also shown. *Bottom panel:* pn (upper) and MOS-summed (lower) spectra extracted from subregion "a" with the corresponding best fit model and residuals ($\chi^2 = 98.8$ with 104 d.o.f.). The best-fit temperatures are $T_{\rm I} = 1.12^{+0.06}_{-0.08} \times 10^6$ K and $T_{\rm II} = 2.7^{+0.3}_{-0.2} \times 10^6$; the best-fit emission measures per unit area are: $N_{\rm I} = 3.0^{+0.4}_{-0.5} \times 10^{18}$ cm^{-5} and $N_{\rm II} = 3.0^{+2}_{-0.6} \times 10^{17}$ cm^{-5}.

brightness. The mean values (over all the subregions) of the temperatures are $1.14 \pm 0.02 \times 10^6$ K (cooler component) and $3.0 \pm 0.1 \times 10^6$ K (hotter component). There are large variations of the emission measure per unit area of the two MEKAL components. Therefore we conclude that the patchy and inhomogeneous morphology of the observed X-ray emission is associated with variations of the extension of the emitting plasma along the line of sight.

Assuming that the temperature of the shocked plasma is mainly determined by the local density, the similarity of the temperatures suggests that the two MEKAL components might be associated with two different phases of the ISM intercepted along the line of sight. Since the emission measures of the two components are not homogeneous in the field of view, they cannot be associated with the inter-cloud medium whose emission is expected to be homogeneous. Therefore the two components may be associated with the inhomogeneities. In particular, we associate the cooler component with the inner and denser part of the clouds (the *core*) and the hotter component with the less dense outer part of the clouds (the *corona*).

3. Shock–cloud interaction

As explained in the previous section, we suggest that the observed X-ray emission is associated with the plasma of the shocked clouds (cloud cores and cloud coronae) and little or no emission from the inter-cloud medium has been detected. Moreover, the lack of inhomogeneities in the plasma temperature and the relationship between optical and X-ray emission, seem to suggest that the reflected shock does not contribute significantly to the X-ray emission.

The two X-ray emission components can then be interpreted as the interaction of the shock with different parts of the clouds. Travelling through different phases of the ISM, the shock heats the plasma at different temperatures, and this generates the X-ray and optical emission, as sketched in Fig. 3. The innermost part of the cloud only emits in the optical band. This part is "embedded" in the core, which is surrounded by the hotter corona. No significant X-ray emission has been detected form the inter-cloud medium. In the figure we report the information we obtained for FilD, representing all the ISM phases intercepted along the line of sight in this region (the values for the optical filaments are taken from Bocchino et al., 2000). The FilD complex can be considered as a structure with an inward increasing density profile and an inward decreasing temperature profile. Fig. 3 shows also that it is reasonable to expect pressure equilibrium between cores and coronae, but that the pressure of these two X-ray emitting phases of the clouds is higher than the inter-cloud pressure. In order to interpret these results, we estimated the radiative and conductive time-scales for the derived values of temperature and density. We found that the thermal conduction between the clouds and the hotter ambient medium is more efficient than radiative cooling. Moreover, if we assume that the efficiency of thermal conduction increases with the temperature (as in the model of Spitzer, 1962), the thermal conduction between inter-cloud medium and clouds is more efficient than the thermal conduction between the X-ray emitting phases of the clouds and the optical filaments. Therefore there is a net heating of cores and coronae and this effect starts up their evaporation in the ambient ISM.

On the other hand, we can see that the pressure of the optically emitting inner part of FilD is significantly lower than the pressure of cores and coronae. This result can be explained considering that in the optical filament,

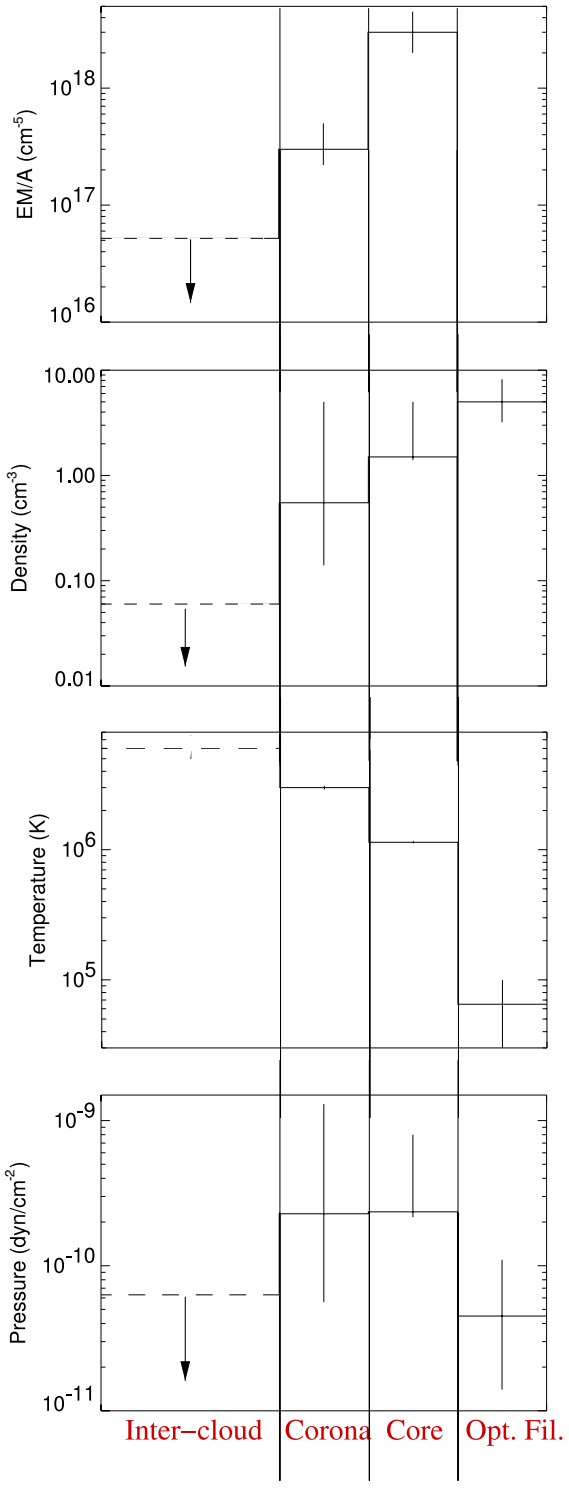

Fig. 3. Schematic view of the FilD post-shock structure. The derived values of emission measure per unit area (in the 0.3–1.1 keV band), particle density, temperature and pressure are reported for the different ISM phases together with their error bars (at 90% confidence level). The values for the optical filament are taken from Bocchino et al. (2000), the inter-cloud temperature has been derived using the Sedov model.

where the temperature is lower and the density is higher, radiative losses govern the evolution of the plasma. Therefore the optical filament loses its thermal energy (and its pressure) through optical and UV emission lines and this cooling produces the collapse of the filament.

As for RegNE, we found that only the hotter component contributes significantly to the observed X-ray emission. The core seems to be nearly absent and no optical filaments are visible. This may indicate that RegNE is a less dense cloud than FilD, but it is also possible that we are observing only the outer part (the corona) of a larger structure that extends beyond the EPIC field of view.

In conclusion, the observed optical and X-ray emission in this region of the Vela SNR are explained by the interaction of the blast-wave shock with the inhomogeneities of the ISM. These inhomogeneities have a complex internal structure and are heated by the transmitted shock which travels through the different phases of the clouds generating an X-ray emission that gets softer as the shock proceeds toward the center of the clouds, where the optical emission originates. Moreover the high efficiency of thermal conduction between the clouds and the hotter inter-cloud medium determines a further heating of the clouds and their evaporation in the ISM.

References

Bocchino, F., Bandiera, R. BeppoSAX observation of the composite remnant G327.1-1.1. A&A 398, 195–202, 2003.

Bocchino, F., Maggio, A., Sciortino, S. ROSAT PSPC observation of the NE region of the Vela supernova remnant. III. The two-component nature of the X-ray emission and its implications on the ISM. A&A 342, 839–853, 1999.

Bocchino, F., Maggio, A., Sciortino, S., Raymond, J. Multi-wavelength observations and modelling of shock–cloud interaction regions in the Vela Supernova Remnant. A&A 359, 316–336, 2000.

Borkowski, K.J., Lyerly, W.J., Reynolds, S.P. Supernova remnants in the sedov expansion phase: thermal X-ray emission. ApJ 548, 820–835, 2001.

Cha, A.N., Sembach, K.R., Danks, A.C. The distance to the Vela supernova remnant. ApJ 515, L25–L28, 1999.

Charles, P.A., Kahn, S.M., McKee, C.F. Einstein observations of selected regions of the Cygnus Loop. ApJ 295, 456–462, 1985.

Fesen, R.A., Blair, W.P., Kirshner, R.P. Spectrophotometry of the Cygnus Loop. ApJ 262, 171–188, 1982.

Graham, J.R., Levenson, N.A., Hester, J.J., Raymond, J.C., Petre, R. An X-ray and optical study of the interaction of the Cygnus Loop supernova remnant with an interstellar cloud. ApJ 444, 787–795, 1995.

Levenson, N.A., Graham, J.R., Hester, J.J., Petre, R. All quiet on the western front? X-ray and optical observations of a prototypical cloud–blast wave interaction in the Cygnus Loop. ApJ 468, 323–329, 1996.

Levenson, N.A., Graham, J.R., Walters, J.L. Dynamic Shocks in the Inhomogeneous Environment of the Cygnus Loop. In: Revista Mexicana De Astronomia Y Astrofisica Conference Series, pp. 252–257, 2003.

Liedahl, D.A., Osterheld, A.L., Goldstein, W.H. New calculations of Fe L-shell X-ray spectra in high-temperature plasmas. ApJ 438, L115–L118, 1995.

Mewe, R., Gronenschild, E.H.B.M., van den Oord, G.H.J. Calculated X-radiation from optically thin plasmas. V. A&AS 62, 197–254, 1985.

Mewe, R., Lemen, J.R., van den Oord, G.H.J. Calculated X-radiation from optically thin plasmas. VI – Improved calculations for continuum emission and approximation formulae for nonrelativistic average Gaunt factors. A&AS 65, 511–536, 1986.

Miceli, M., Bocchino, F., Maggio, A., Reale F. Shock–cloud interaction in the Vela SNR observed with XMM-Newton. A&A (submitted for publication).

Miyata, E., Tsunemi, H. Reflection-shocked Gas in the Cygnus Loop Supernova Remnant. ApJ 552, 624–638, 2001.

Patnaude, D.J., Fesen, R.A., Raymond, J.C., et al. An isolated, recently shocked ISM cloud in the Cygnus Loop Supernova Remnant. AJ 124, 2118–2134, 2002.

Spitzer, L. Physics of Fully Ionized Gases, second ed. Interscience, New York, 1962.